PVDF-based photoacoustic spectroscope for the identification of clathrates

*Thomas Stahl[1], Thomas Allen[2], James Guggenheim[2] and Paul Beard[2]

[1] *German Engineering Research and Development Center LSTME Busan, Busan 46742, Korea*
[2] *Department of Medical Physics and Biomedical Engineering, University College London, London WC1E 6BT, United Kingdom*
*stahl.thomas@yahoo.com

ABSTRACT

Clathrate technologies have gained increased attention, both in industry and the research community, owing to their applicability in various fields, such as gas storage, water desalination and wastewater treatment. Novel applications, such as applying clathrates for the concentration of fruit juices, have recently been reported.
In this paper we present a novel method based on photoacoustic spectroscopy for the analysis of clathrates in aqueous environments. This self-referencing method poses a simple and robust approach, determining the formation of clathrates and identifying the guest molecule contained within the clathrate via the measurement of the Grüneisen coefficient using a PVDF-based photoacoustic spectroscope. The method presented holds high potential for industrial applications of clathrates since it has the potential to help saving time, energy and resources during the clathrate forming process via *in situ* measurements.

1. INTRODUCTION

A clathrate is a chemical material consisting of a cage-like matrix, often made up from water molecules, which entrap a guest molecule. They are found in nature, for example in sediments in permafrost regions and in the deep sea, and can, under specific conditions, be generated synthetically - synthetic clathrates. One technical problem related to formation of clathrate is the blockage of offshore gas pipelines. Due to the high pressure in those systems clathrates have been forming in the pipes to that extend, that the pipes have been blocked, causing leaks and the subsequent release of potent greenhouse gases, such as methane, transported through those pipes. This complication has fueled the research in the field of clathrates and accelerated the investigation in discovering the interaction between water and the clathrate formation of natural gasses. However, due to their structure and composition, synthetic clathrates have found numerous industrial applications where their formation is desired. Accordingly, synthetic clathrates have been employed for the selective separation of compounds from mixtures of gases, liquids and solids. Today clathrate technology is

being employed in a variety of industrial applications in fields such as food processing[1,2], energy storage[3], wastewater treatment[4] and drinking water preparation[5]. Another application of synthetic clathrates that has been proposed is the purification and separation of the components of air[6]. The formation of synthetic clathrates requires elevated pressures and decreased temperatures, which can be relatively energy demanding. However, if analyzed *in situ* the energy consumption for the phase transition step has potential for optimization.

In the past, clathrates have been analyzed by means of gas chromatography[8], Raman spectroscopy[9], X-ray diffractometry[10], particle size analysers[11], nuclear magnetic resonance[12] and infrared spectroscopy[13]. Spectroscopic technologies enable measuring the physical properties of the clathrates, such as their crystal structure, gas composition and analyze the clathrate composition in situ, without decomposing the sample.

Based on the photoacoustic (PA) effect, PA spectroscopy is a spectroscopy modality which has been employed for the analysis of gaseous, liquid and solid samples. The PA effect denotes the generation of acoustic pressure waves in matter (solids, liquids and gases) upon the exposure to modulated light or short light pulses. The pressure waves generated via the PA effect can be detected by means of an acoustic transducer. Monitoring the pressure waves at different wavelengths has been termed PA spectroscopy. This measurement technique has been utilized previously in various fields of applications, such as environmental monitoring[14], forensic sciences[15], biological[16] and biomedical[17] analysis, as well as chemical reaction monitoring[18]. Depending on the state of the sample the transduction method of PA spectroscopy differs. In the case of a gaseous sample modulated continuous light sources are used routinely for the excitation and resonant gas cells are utilized for sample containment. This technique relies on the indirect detection of heat generated by nonradiative relaxations of an excited state of the absorbing molecules contained in the sample. This causes a change of the gas pressure which can be detected by means of a microphone. For the PA analysis of a liquid sample however, pulsed lasers are used as the excitation light source. After excitation of the light by a sample an ultrasound is generated by the non-radiative relaxation of the sample molecules and the generated ultrasound is detected by a microphone. PA spectroscopy shows high potential as an analytical modality due to its high sensitivity (for gas analysis often quoted with a detection limit as low as ppbV up to sub pptV[14]) within a large dynamic range, robustness, ease of use, good temporal resolution, versatility, multicomponent capability and insensitivity to light scattering. In addition to the identification and quantification of gases, PA spectroscopy has the potential to identify and characterize clathrates due to their alternated capability of converting heat energy to an acoustic pressure, also known as Grüneisen efficiency (Γ), compared to the pure components of the clathrate. Since this has not been shown before, the present study details a polyvinylidene fluoride (PVDF) based PA spectroscopy set up which allows for the estimation of the wavelength-specific absorption coefficient, PA amplitude and Γ of a liquid sample. After the description of the PA spectroscope and its limitations, a method enabling the identification of clathrates in an aqueous system is presented and verified. The method provided is self-referencing and offers a robust approach for the determination of clathrate formation.

2. MATERIALS AND METHODS

<u>Photoacoustic spectroscope</u>

The experimental arrangement described in the following, termed PA spectroscope, was used throughout this study for the measurement of the PA amplitude and μ_a spectra, allowing for the determination of Γ of the sample solutions. A schematic of the PA spectroscope is depicted in Fig. *1*.
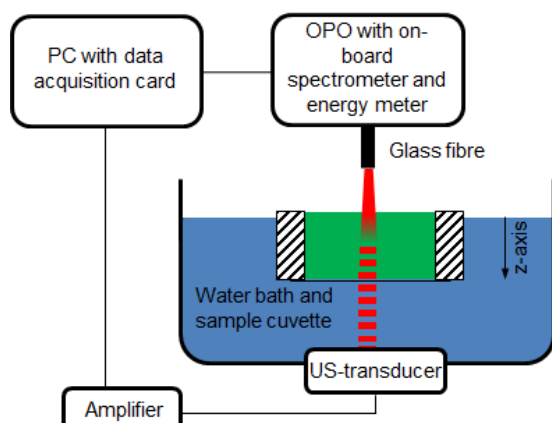

Fig. 1: Schematic of the PA spectroscope used for the determination of PA amplitude and μ_a spectra.

For the excitation of the samples and the subsequent generation of the ultrasonic signals an Nd:YAG pumped optical parametric oscillator (OPO) laser system (Spitlight 600, Innolas Laser GmbH, Germany) tunable from 420-2500 nm with a pulse length of <8 ns was employed. For the measurement of the relative output power of the laser and the emitted wavelength the laser system is equipped with a power meter and a spectrometer, respectively. The optical output of the laser system was coupled via a fused silica optical fiber with a diameter of 1.5 mm and guided towards the sample contained in a sample cuvette. The sample cuvette consists of a block of Perspex with side length of 45 x 35 mm^2 and a height of 15 mm with a drilled hole (20 mm in diameter) in the center of it. A polyethylene film with a thickness of 50 μm was cemented to the bottom of the Perspex block sealing the drilled hole and allowing to introduce a maximum sample volume of about 3 ml. For the measurements the sample cuvette is placed in the laser light beam in a water tank, with the drilled hole centered above the ultrasound transducer. The ultrasound transducer base consists of a Perspex block with a side length of 45 x 35 mm^2 and a height of 10 mm, which is mounted to a window in the bottom of the water tank and seals the water tank by means of a square rubber gasket. For the active material a PVDF film with a thickness of 52 μm and a side length of 10 x 10 mm^2 was chosen. The ultrasound transducer demonstrated a noise equivalent pressure of 1.9 kPa over a 20 MHz bandwidth and a -

3 dB bandwidth of 18.5 MHz and is electrically connected via a low noise voltage amplifier (HVA-200M-40-F, Femto, Germany) to a data-acquisition card (PCIe6323, National Instruments) for digitization of the analogue signal and to enable downloading of the time-resolved data to a PC. Labview was employed to control the laser and to record the readings from the laser onboard power meter, spectrometer and the PVDF transducer connected via the amplifier.

From each of the detected PA signals two parameters were extracted: i) the peak signal amplitude ($S(\lambda)_{0,Measurement}$) and ii) μ_a. The two parameters were determined as shown in Fig. 2.
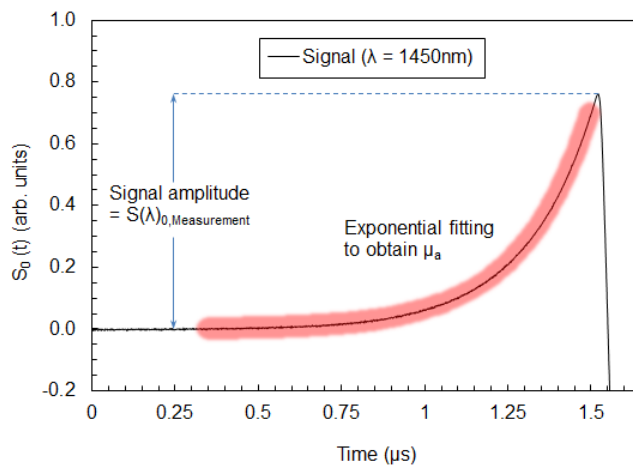

Fig. 2: Time-resolved PA signal generated using water as a chromophore (black line) at an excitation wavelength of 1450 nm. The part of the signal marked in red is the part of the signal used for the determination of μ_a. $S(\lambda)_{0,Measurement}$ was obtained as indicated by the blue arrows.

In order to obtain μ_a, the analytical expression Eq. (1) was fitted to the initial compressive part of the measured PA signal (for $t < t_0$).

$$\text{(1)} \qquad S_0(t) = \Phi_0\, \mu_a\, e^{-(\mu_a\, c_s\, (t - t_0))}\, E_t\, \Gamma\, K$$

Φ_0 is the initial fluence, c_s is the speed of sound in the medium, t_0 is the time at which the signal amplitude is at its maximum, E_t is the thermalization efficiency of the chromophore and K is a scaling factor accounting for the acoustic sensitivity of the set up.

The relative laser power, $O(\lambda)_{Measurement}$, was measured for each wavelength during signal acquisition in order to correct the measured PA amplitude, $S(\lambda)_{0,Measurement}$, for the wavelength dependence of the fluence using Eq. (2).

$$\text{(2)} \qquad S_0(\lambda) = \frac{S(\lambda)_{0,Measurement} \cdot O(\lambda)_{Calibration}}{M(\lambda)_{Calibration} \cdot O(\lambda)_{Measurement}}$$

$O(\lambda)_{Calibration}$ is the light energy measured with the light energy measured with the laser onboard power meter and $M(\lambda)_{Calibration}$ is the light energy measured using an external power meter (Fieldmax II, Coherent, CA, USA) mounted at the fiber tip, replacing the sample cuvette. Both parameters ($O(\lambda)_{Calibration}$ and $M(\lambda)_{Calibration}$) were acquired in a separate calibration step.

Determination of Γ

For the determination of the Γ of a sample solution, consisting of a sample chromophore and a solvent, two PA signals are acquired. One signal is generated at a wavelength, λ_s, at which the absorption of the solvent is negligible, and the sample chromophore exhibits strong absorption and therefore solely depends on the properties on the sample chromophore. The S_0 of the signal generated in the sample at t_0 is given by Eq. (3).

$$(3) \qquad S_{0,s} = \Phi_0\, \mu_{a,s}\, E_{t,s}\, \Gamma_s\, K$$

$S_{0,s}$ is the signal amplitude of the sample chromophore at t_0 and λ_s, $\mu_{a,s}$ is the absorption coefficient of the sample chromophore, $E_{t,s}$ is the thermalization efficiency of the sample chromophore and Γ_s is the Grüneisen coefficient of the sample chromophore.

The second signal is generated at a wavelength, λ_r, at which the absorption of the sample chromophore is negligible, and the solvent exhibits strong absorption, here denoted as the reference signal. S_0 at t_0 and λ_r for the reference is given by Eq. (4).

$$(4) \qquad S_{0,r} = \Phi_0\, \mu_{a,r}\, E_{t,r}\, \Gamma_r\, K$$

Here $S_{0,r}$ is the signal amplitude of the reference at t_0 and λ_r, $\mu_{a,r}$ is the absorption coefficient of the reference, $E_{t,r}$ is the thermalization efficiency of the reference and Γ_r is the Grüneisen coefficient of the reference. If Γ_r and $E_{t,r} = E_{t,s}$ are known, Γ_s can be calculated using Eq. (5).

$$(5) \qquad \Gamma_s = \frac{S_{0,s}/\mu_{a,s}}{S_{0,r}/\mu_{a,r}}\, \Gamma_r$$

The ability of the method for determining Γ was tested using two sample chromophores, ethanol and methanol. The sample solutions were made up from mixtures of the sample chromophores in water at different concentrations. The two alcohols were chosen because their E_t can reasonably be assumed to be 1 and their Γ_s can be obtained using thermodynamic data found in literature using Eq. (6).

(6)
$$\Gamma = \frac{\beta c_s^2}{c_p}$$

Here β is the volume thermal expansion coefficient, c_s is the sound speed and c_p is the heat capacity at constant pressure. $\Gamma_r = 0.12$ for water as a reference chromophore was obtained from literature[19]. The results of the measurements (data not shown) display the expected decrease of Γ with increasing water content, following a linear trend with high correlation ($R^2 = 0.993$ and $R^2 = 0.9865$ for methanol and ethanol respectively) and low standard deviation (less than 5% throughout the whole measurement range). Extending linear trend lines towards a water content of 100% shows that both lines intercept roughly with the literature value of water at about $\Gamma_r = 0.12$. The measured and calculated values of Γ_s for the pure alcohols are in close agreement with the values calculated using Eq. (6) (0.47 (+/- 4%) and 0.48 for methanol and 0.60 (+/- 2%) and 0.61 for ethanol). These results demonstrate, that the method proposed allows for the accurate determination of Γ of liquids such as methanol and ethanol. Furthermore, if a linear trend of Γ of mixtures of the alcohol with varying water content can be assumed, the method enables the estimation of Γ of mixtures of liquids. In order to further demonstrate the method for the determination of Γ, solutions of various concentrations of either copper chloride ($CuCl_2$; 70-430 gL^{-1}) or nickel chloride ($NiCl_2$; 250-480 gL^{-1}) were prepared and analyzed as described in above. $CuCl_2$ and $NiCl_2$ were chosen for these experiments due to their concentration dependence of Γ, which follows a linear trend as demonstrated previously[20]. The results of the measurements are shown in Fig. 3.
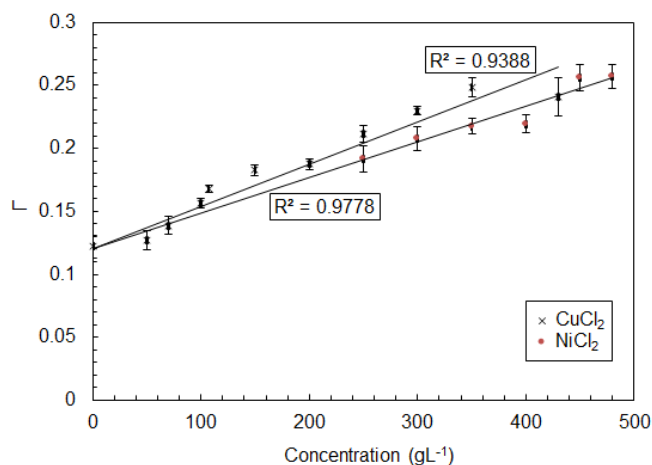

Fig. 3: Γ versus the concentration of $CuCl_2$ (black crosses) and $NiCl_2$ (red dots) in water and Γ of pure water.

As expected, Γ increases with increasing salt concentration. The measured values align with the linear trend lines originating from $\Gamma = 0.12$ with R^2 values of 0.9388 and 0.9778 for $CuCl_2$ and $NiCl_2$, respectively. The standard deviation of the values range from 2-11% and are high for $NiCl_2$ due to its low extinction coefficient and therefore low signal to noise ratio of the PA signal, even at the high concentrations measured. The

measurements at the concentrations >400 gL^{-1} using $CuCl_2$ and $NiCl_2$ show increased standard deviations and decreased accuracy. This is thought to be due to the limited bandwidth of the acoustic transducer used for the detection of the PA signals resulting in less accurate determination of the PA amplitude and μ_a, leading to a higher standard deviation and error of the calculated Γ. The increased standard deviation in the lower concentration range for both of the salt solutions can be assigned to low signal to noise ratio due to low absorption coefficients.

3. RESULTS

Identification of Clathrates

After validating the method for the determination of Γ of various sample solutions, it was investigated if a mixture of chromophores with separate absorption bands may exhibit different efficiencies converting heat to stress and therefore exhibit a wavelength dependence of Γ. An example where this effect may be observed are gold nanoparticles with varying coatings such as gold nanoparticles covered in a silica shell compared to plain gold nanoparticles. It has been shown that the silica coating alters the thermal coupling of the nanoparticles and therefore alters Γ[21]. If the two species of gold nanorods would exhibit separate absorption bands, the measurement of Γ of a mixture of the two nanoparticle species may demonstrate wavelength dependence. Another example where this might be observed is a mixture of nanoparticles and organic dyes or other chromophores.

In order to analyze the wavelength dependence of Γ of a sample mixture, various solutions of chromophores were studied. Initially, to investigate this, the Γ spectrum of a solution of an organic dye (IR 820) dissolved in water at a concentration of 400 µM was determined. In order to generate the Γ spectrum, initially Γ was determined at λ_{max} of IR 820 (820 nm) as described above. Next, the ratio of PA amplitude to μ_a at each wavelength of the measured wavelength range was calculated, normalized to the value at λ_{max} and multiplied by Γ calculated for λ_{max}. The results are shown in Fig. 4.
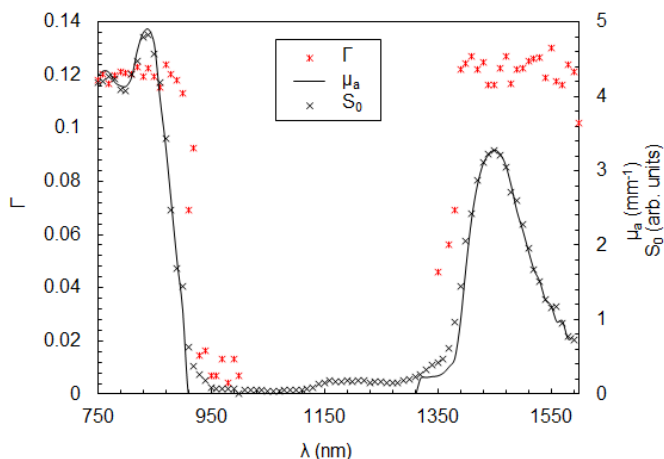
Fig. 4: Γ (red stars), PA amplitude (black crosses) and μ_a (black line) spectra of IR 820 measured using the PA spectroscope.

Fig. 4 shows that in the wavelength range from 750-880 nm and 1390-1590 nm Γ is relatively constant. The deviation from the value of Γ of water (Γ(H2O) = 0.12) is no more that 7% over this wavelength range. Strong deviations from this constant value of Γ can be observed in the wavelength range from 880-1390 nm. These values are measurement errors due to a low signal to noise ratio. A constant Γ for a sample consisting of the sample mixture consisting of organic dye with water as solvent was expected because the ability to convert the heat energy to an acoustic pressure of a dye molecule (as the light absorbing species) in water is assumed to be identical compared to a water molecule (as the light absorbing species).

Next, in order to further analyze the possibility of a wavelength dependence of Γ, aqueous solutions of $CuCl_2$ were employed because the salt is known to alter the value of Γ of a solution as shown in Fig. 3. Water was used as the second chromophore in the mixture, consistent with the previous experiment. Γ spectra of the mixture were generated at room temperature and at 4 °C in order to evaluate the influence of the reduced thermal expansion coefficient of water at this temperature on the measured Γ. The PA amplitude, μ_a and Γ spectra generated at the two temperatures are shown in Fig. *5*.
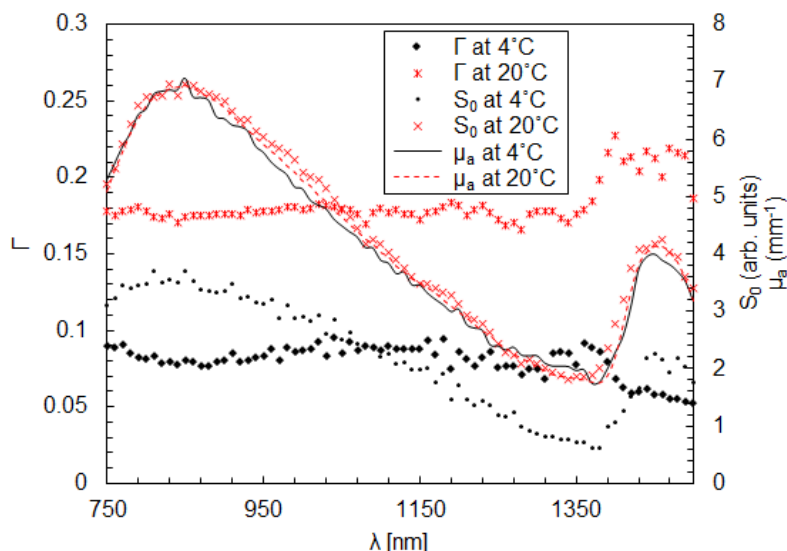
Fig. 5: PA amplitude (red crosses), μ_a (red dashed line) and Γ (red stars) spectra of CuCl$_2$ (200 gL^{-1}) in water at 20 °C compared to PA amplitude (black crosses), μ_a (black line) and Γ (black squares) spectra of CuCl$_2$ (200 gL^{-1}) in water at 4 °C.

The resulting PA amplitude and the μ_a spectrum at 20 °C agree well with each other and the μ_a spectrum at 4 °C. However, the PA amplitude at 4 °C is reduced by about 50% at the wavelength of peak absorption of the salt (850 nm) and the solvent (1450 nm). Minor differences in amplitude and shape of the μ_a spectrum can be attributed to low signal to noise ratio generated at the lower temperatures. The difference in the PA amplitude at the two temperatures can be explained with the decreased Γ at the lower temperatures - at 4 °C Γ(CuCl$_2$) = 0.08 compared to Γ(CuCl$_2$) = 0.17 at room temperature. However, the calculated Γ values show spectral features, especially near the absorption maxima of the solvent from about 1380-1500 nm. Comparing Γ in the spectral range of 750-1370 nm to Γ in the spectral range from 1380-1500 nm shows a change in the amplitude of the values differing by 14% and 20% at room temperature and at 4 °C, respectively. Additional to the feature at the peak absorption of the solvent, a subtle dip around λ_{max} of the metal ion (Cu^{2+}) around 820 nm is apparent.

To further investigate these spectral features of Γ, CuCl$_2$ was dissolved in the organic solvents water and isopropanol, in order to exploit the different values of Γ of the solutions produced. Subsequently, PA amplitude, μ_a and Γ spectra of the different samples were generated and the resulting spectra were overlaid as shown in Fig. 5. In addition to this the PA amplitude spectra of the pure solvent were generated for comparison. The results are shown in
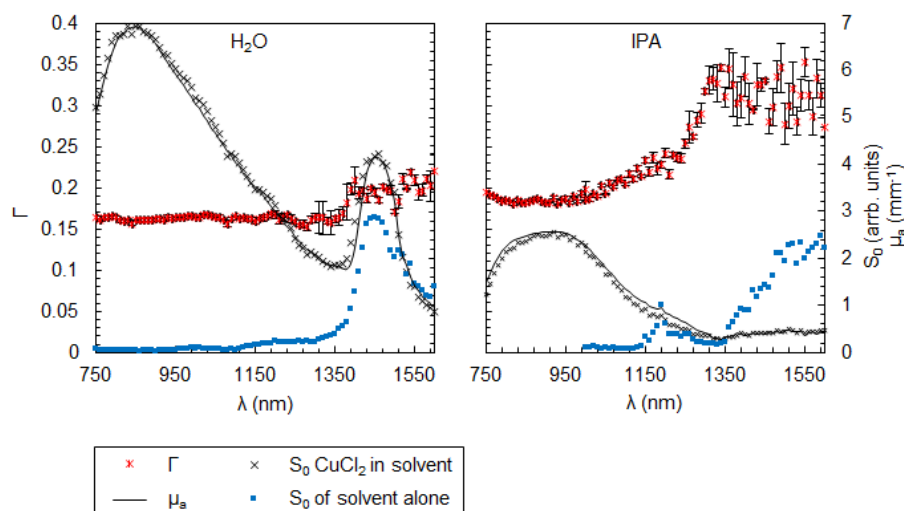Fig. *6.*

Fig. 6: Γ (red stars), PA amplitude (black crosses) and a (black line) spectra of the $CuCl_2$ solutions using various solvents and PA amplitude spectra of the pure solvents used for the experiments (blue squares). The solvents used were water (H_2O) and isopropanol (IPA).

The change in the wavelength of maximum absorption of $CuCl_2$ is due to the variable electronic environment provided by the solvents of Cu^{2+}. The trend of the spectral features of Γ, such as the increased Γ with increased influence of the solvent (for the aqueous sample at $\lambda > 1400nm$ and for the sample using isopropanol as a solvent at $\lambda > 1300nm$) compare well to the features indicated in Fig. 5Fig. *6*. Particularly striking is the increased Γ at wavelength between 1300 and 1600 nm in the measured range. Γ of the isopropanol/$CuCl_2$ mixture changes by about 50% from the minimum ($\Gamma(820 \text{ nm}) = 0.27$) to the maximum ($\Gamma(1550 \text{ nm}) = 0.53$) value. Another feature of the isopropanol/$CuCl_2$ Γ spectrum is the dip around λ_{max} of the metal ion at 820 nm, which also can be made out for the Γ spectrum of copper ions at 4 °C in the range between about 750-950 nm shown in Fig. 5.

4. CONCLUSION

The change of Γ with wavelength and its spectral features can possibly be explained by considering the behavior of ions in solution, such as copper, nickel or chlorine ions in aqueous solution or in an organic solvent. For example, when dissolved in an aqueous solution, $CuCl_2$ is solvated by the water molecules forming copper (Cu^{2+}) and two chlorine ions (Cl^-), which are solvated by a number of water molecules forming clusters which are called clathrates. A clathrate consists of an atom or molecule which is trapped by other molecules. A scheme of an example of a clathrate, consisting of a hydrated metal ion, is shown in Fig. 7.
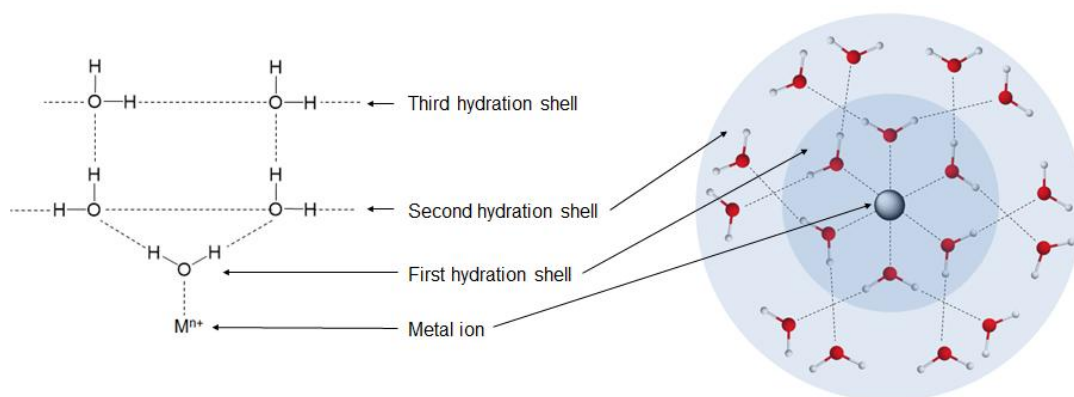
Fig. 7: Scheme of the hydrogen bonding pattern in the first three hydration shells (left) and an example of a metal ion trapped by water molecules (right). The red spheres in the scheme on the right represent oxygen atoms, the white spheres hydrogen atoms and the grey spheres the metal ion. Dashed lines represent hydrogen bonds.

A well-known example of a clathrate is the methane clathrate, also known as frozen methane. The clathrates consist of methane molecules trapped by hydrogen bonded water molecules. Another example is clathrates consisting of ions trapped by solvent molecules. The process of entrapping ions by the solvent molecules is called solvation or, in the case of water as a solvent, hydration. The influence of an ion in solution on the solvent depends on factors such as size and charge of the ion[22]. It has been proposed, that an ion can influence solvent molecules in a range of up to several hundreds of nanometres, involving 103-108 solvent molecules[23] in layers (in aqueous solution called hydration shells) around the central ion, resulting in an increased local density of solvent molecules around the ions compared to the rest of the bulk solution. The solvent molecules are affected in various ways, such as induced charge transfer, changing of the dipole orientation and distorting of the hydrogen-bond network in the bulk[24]. The effects of these interactions are predominant in the first hydration shell and can be observed by the elongation of the oxygen lone pair orbitals along the ion-oxygen direction and the influence on the hydrogen bonding electrons, resulting in a strong polarization of the molecules[25]. In addition, recently, Ahmed *et al* were able to show that the water molecules involved in formation of the hydration shell are vibrationally decoupled from their neighboring bulk water molecules[26]. These properties of clathrates may be the reason for the observed wavelength dependency of Γ of the solutions (Cu^{2+} ions in various solvents). In particular the increased local density of solvent molecules surrounding the central ion of a clathrate compared to the bulk solution might explain the observed wavelength dependence of Γ, because the density has a direct influence on Γ via

$$(7) \qquad \Gamma = \frac{\beta \, K_s}{c_p \, \rho}$$

where K_s is the adiabatic bulk modulus and ρ is the density. As a result of the changed local density due to the formation of clathrates, the two absorbing species (Cu^{2+} and

the solvent) in the spectral region measured (750-1500 nm), exhibit different efficiencies converting heat to stress as shown by plotting the Γ spectra. At about 4 °C the density of water is at its maximum and the thermal expansion at its minimum. At this temperature (4 °C), Cu^{2+} clathrates are more efficient converting the thermalized energy to stress than the bulk water. The effect can be observed in Fig. 5, showing the increased Γ values in the spectral region around the clathrate absorption peak (750-1300 nm) compared to the spectral region around the solvent absorption peak (1350-1500 nm) at 4 °C. However, at 20 °C the thermal expansion of water is increased and thus the conversion from heat to stress is more efficient, shown by the values of Γ in the spectral region from 1350-1500 nm. Even though the spectral features of Γ are in the same position, the amplitude of the measurements of Γ at 4 °C differs significantly from the measured Γ at 20 °C. At 20 °C the average Γ of the aqueous Cu^{2+} solution is increased due to the increased thermal expansion of water. However, apart from the changing amplitude, a blue shift of the maximum Γ by more than 500 nm is noticeable. In the case of the solution at 4 °C the efficiency of the bulk water to convert heat to stress is lower compared to the ability of the clathrates. At increasing temperatures, the situation is reversed and at 20 °C the amplitude is greater around the water absorption peak (1450 nm) than around the ion absorption peak (850 nm). It can therefore be concluded that the conversion from heat to stress is more efficient in the bulk water compared to the Cu^{2+} clathrates at increased temperatures. The same holds true for solutions of $CuCl_2$ in organic solvents. Fig. 6 shows the Γ spectrum measured using $CuCl_2$ in water and isopropanol. The spectral features of Γ shown are comparable to those identified in Fig. 5 and can also be explained by the formation of clathrate like structures. These structures and the bulk solvent exhibit a different efficiency converting heat to stress likely to be caused by the increased local density of solvent molecules surrounding the metal ions compared to the bulk solvent. Another feature presented in Fig. 6 is the small intermediate peak in the Γ spectra of the isopropanol/$CuCl_2$ mixture at about 1200 nm, which is due to the increased influence on Γ of the solvent, caused by the absorption peak of isopropanol in this spectral region. At wavelengths where both absorbing species pose significant absorption, the values of Γ depends on both species and thus introduces features such as the intermediate peak at around 1200 nm in the Γ spectrum of Cu^{2+} in isopropanol.

In conclusion, the present study describes a method based on time-resolved PA spectroscopy for the identification of clathrates in liquid media. The method relies on the measurement of Γ of the two species within the sample - the solvent and the clathrate. The altered Γ can be attributed to a different local density of the molecules making up the clathrate cage compared to the bulk solvent molecules. This method poses a robust and simple alternative to existing methods and has the potential to promote the industrial use of hydrates via reducing the energy consumption for the hydrate formation.

REFERENCES

1. Seidl P, Loekman S, Sardogan M, et al. Food technological potentials of CO 2 gas hydrate technology for the concentration of selected juices. *High Press Res.*

2019;39(2):344-356. doi:10.1080/08957959.2019.1597077

2. Li S, Shen Y, Liu D, Fan L, Tan Z. Concentrating orange juice through CO_2 clathrate hydrate technology. *Chem Eng Res Des*. 2015;93:773-778. doi:10.1016/j.cherd.2014.07.020

3. Veluswamy HP, Kumar A, Seo Y, Lee JD, Linga P. A review of solidified natural gas (SNG) technology for gas storage via clathrate hydrates. *Appl Energy*. 2018;216:262-285. doi:10.1016/j.apenergy.2018.02.059

4. Song Y, Dong H, Yang L, et al. Hydrate-based heavy metal separation from aqueous solution. *Sci Rep*. 2016;6(1):21389. doi:10.1038/srep21389

5. Babu P, Nambiar A, He T, et al. A Review of Clathrate Hydrate Based Desalination To Strengthen Energy–Water Nexus. *ACS Sustain Chem Eng*. 2018;6(7):8093-8107. doi:10.1021/acssuschemeng.8b01616

6. Kang S-P, Lee H. Recovery of CO 2 from Flue Gas Using Gas Hydrate: Thermodynamic Verification through Phase Equilibrium Measurements. *Environ Sci Technol*. 2000;34(20):4397-4400. doi:10.1021/es001148l

7. Tajima H, Yamasaki A, Kiyono F. Energy consumption estimation for greenhouse gas separation processes by clathrate hydrate formation. *Energy*. 2004;29(11):1713-1729. doi:10.1016/j.energy.2004.03.003

8. Bhattacharyya AC, Bhattacharjee A. Gas-chromatographic investigation on clathrate-forming transition metal complexes. *Anal Chem*. 1969;41(14):2055-2058. doi:10.1021/ac50159a044

9. Uchida T, Takeya S, Wilson LD, et al. Measurements of physical properties of gas hydrates and in situ observations of formation and decomposition processes via Raman spectroscopy and X-ray diffraction. *Can J Phys*. 2003;81(1-2):351-357. doi:10.1139/p03-017

10. Takeya S, Shimada W, Kamata Y, et al. In Situ X-ray Diffraction Measurements of the Self-Preservation Effect of CH 4 Hydrate. *J Phys Chem A*. 2001;105(42):9756-9759. doi:10.1021/jp011435r

11. Clarke MA, Bishnoi PR. Determination of the intrinsic kinetics of CO_2 gas hydrate formation using in situ particle size analysis. *Chem Eng Sci*. 2005;60(3):695-709. doi:10.1016/j.ces.2004.08.040

12. Gao S, House W, Chapman WG. NMR/MRI Study of Clathrate Hydrate Mechanisms. *J Phys Chem B*. 2005;109(41):19090-19093. doi:10.1021/jp052071w

13. Dartois E, Deboffle D, Bouzit M. Methane clathrate hydrate infrared spectrum. *Astron Astrophys*. 2010;514:A49. doi:10.1051/0004-6361/200913642

14. Tomberg T, Vainio M, Hieta T, Halonen L. Sub-parts-per-trillion level sensitivity in trace gas detection by cantilever-enhanced photo-acoustic spectroscopy. *Sci Rep*. 2018;8(1):1848. doi:10.1038/s41598-018-20087-9

15. El-Sharkawy YH, Elbasuney S. Novel laser induced photoacoustic spectroscopy for instantaneous trace detection of explosive materials. *Forensic Sci Int*. 2017;277:215-222. doi:10.1016/j.forsciint.2017.06.005

16. Pontes MS, Grillo R, Graciano DE, et al. How does aquatic macrophyte Salvinia auriculata respond to nanoceria upon an increased CO_2 source? A Fourier transform-infrared photoacoustic spectroscopy and chlorophyll a fluorescence study. *Ecotoxicol Environ Saf*. 2019;180:526-534.

doi:10.1016/j.ecoenv.2019.05.041

17. Dumitras DC, Dutu DC, Matei C, et al. Evaluation of ammonia absorption coefficients by photoacoustic spectroscopy for detection of ammonia levels in human breath. *Laser Phys.* 2011;21(4):796-800. doi:10.1134/S1054660X11070061

18. Morales-Rodriguez ME, McFarlane J, Kidder MK. Quantum Cascade Laser Infrared Spectroscopy for Online Monitoring of Hydroxylamine Nitrate. *Int J Anal Chem.* 2018;2018:1-9. doi:10.1155/2018/7896903

19. Yao D-K, Zhang C, Maslov K, Wang L V. Photoacoustic measurement of the Grüneisen parameter of tissue. *J Biomed Opt.* 2014;19(1):017007. doi:10.1117/1.JBO.19.1.017007

20. Laufer J, Zhang E, Beard P. Evaluation of Absorbing Chromophores Used in Tissue Phantoms for Quantitative Photoacoustic Spectroscopy and Imaging. *IEEE J Sel Top Quantum Electron.* 2010;16(3):600-607. doi:10.1109/JSTQE.2009.2032513

21. Chen Y-S, Frey W, Aglyamov S, Emelianov S. Environment-Dependent Generation of Photoacoustic Waves from Plasmonic Nanoparticles. *Small.* 2012;8(1):47-52. doi:10.1002/smll.201101140

22. Bock CW, Markham GD, Katz AK, Glusker JP. The Arrangement of First- and Second-shell Water Molecules Around Metal Ions: Effects of Charge and Size. *Theor Chem Acc.* 2006;115(2-3):100-112. doi:10.1007/s00214-005-0056-2

23. Sedlák M. Large-Scale Supramolecular Structure in Solutions of Low Molar Mass Compounds and Mixtures of Liquids: I. Light Scattering Characterization. *J Phys Chem B.* 2006;110(9):4329-4338. doi:10.1021/jp0569335

24. Chen Y, Okur HI, Gomopoulos N, et al. Electrolytes induce long-range orientational order and free energy changes in the H-bond network of bulk water. *Sci Adv.* 2016;2(4):e1501891. doi:10.1126/sciadv.1501891

25. Krekeler C, Delle Site L. Lone pair versus bonding pair electrons: The mechanism of electronic polarization of water in the presence of positive ions. *J Chem Phys.* 2008;128(13):134515. doi:10.1063/1.2873768

26. Ahmed M, Namboodiri V, Singh AK, Mondal JA. On the intermolecular vibrational coupling, hydrogen bonding, and librational freedom of water in the hydration shell of mono- and bivalent anions. *J Chem Phys.* 2014;141(16):164708. doi:10.1063/1.4899070